2016

INFLUENCE OF THE WEATHERED LAYER ON RETRIEVING BODY WAVE USING PASSIVE SIESMIC INTERFEROMETRY

Boming Wu
Michigan Technological University, bomingw@mtu.edu

INFLUENCE OF THE WEATHERED LAYER ON RETRIEVING BODY WAVE USING PASSIVE SIESMIC INTERFEROMETRY

By

Boming Wu

A THESIS

Submitted in partial fulfillment of the requirements for the degree of

MASTER OF SCIENCE

In Geological Engineering

MICHIGAN TECHNOLOGICAL UNIVERSITY

2016

This thesis has been approved in partial fulfillment of the requirements for the Degree of MASTER OF SCIENCE in Geological Engineering.

Department of Geological and Mining Engineering and Sciences

Thesis Co-Advisor: *Wayne D. Pennington*

Thesis Co-Advisor: *Roohollah Askari*

Committee Member: *Roger M. Turpening*

Department Chair: *John S. Gierke*

Table of contents

List of Figures

Abstract

Passive seismic interferometry (SI) is an increasingly popular seismic method due to its cost-efficient advantage because it does not need an active source. Techniques in using SI to retrieve surface waves are relatively well established, but using SI to retrieve body waves is still under development by many authors. These geophysicists have proved that many factors, such as average duration of the natural sources, the number of natural sources that occurred during recording time, source distribution, etc., influence the quality of body waves retrieved. In this research, I focus on how to make use of the attenuation property of weathered layers to weaken the negative impact of surface noise. First, I model the negative effects of surface noise. Then, I test the effect of burying the receivers in order to improve the retrieved body waves. Finally, I discuss some solutions for removing multiples reflected from free surface.

1. Introduction

Seismic interferometry is an unconventional seismic method developed in this century. It refers to a method of retrieving Green's function from any two points under some certain restrictions. These two points could be a source and a receiver, two sources (Curtis, 2009), or two receivers (Wapenaar, 2004; van Manen et al., 2005, 2006; Snieder et al., 2006). This concept was first proposed by Claerbout (1968), who found that the autocorrelation of a trace on tracing a signal from depth arriving at a surface receiver is equal to the surface receiver having recorded the signal from a surface source. From this one-dimensional model, Clearbout then derived the Green's functions in the three-dimensional case. In the three-dimensional scheme, "by crosscorrelating noise traces recorded at two locations on the surface, we can construct the wave field that would be recorded at one of the locations if there was a source at the other." (Rickett and Claerbout, 1999; later verified by Wapenaar, 2003). Thereafter, some geophysicists devoted effort to extend this concept to random media (Weaver and Lobkis, 2001; van Tiggelen, 2003; Snieder, 2004).

In the time since this three-dimensional scheme was proposed, more geophysicists have become involved in applying this method to real seismic data. Scherbaum (1987) explored the subsurface site structure using seismic interferometry in Swabian Jura,

Southwest Germany. Rickett and Claerbout (1999) applied this method to daylight imaging.

Time lapse seismic surveys provide an effective way to detect subsurface changes. The conventional way to acquire time lapse seismic data is to use active sources to get information reflected form subsurface. During the past decade, passive seismic interferometry has been used more widely in time lapse monitoring. Boullenger et al. (2015) applied passive seismic interferometry method on 4D time-lapse survey. Compared with the conventional active method, seismic interferometry uses long-term (or permanently) installed seismic stations, making the repeatability of the survey more efficient and reliable.

Seismic interferometry includes controlled source data (Bakulin and Calvert, 2006), and passive seismic data (Draganov et al., 2006; Forghani and Snieder, 2010). For passive seismic data, using natural sources to retrieve surface wave has been well established (Campillo and Paul, 2003; Shapiro and Campillo, 2004), but retrieving reflected body waves has been successful only recently (Draganov et al., 2007, 2009). In general, retrieving body waves remains doubtful and the retrieved quality is poor.

To test new ideas for obtaining body wave, Thorbecke and Draganov (2011) developed an open source numerical code – 2D Finite-Difference Wave-field

Modelling. In their paper, they discussed some of the factors that influence the quality of the retrieved reflections: duration and number of passive sources present during the recording time, source distribution, source strength, the presence of intrinsic attenuation in the medium, and the effect of receiver topography. Draganov et al. (2004) also discussed the influence of clustered noise sources on the result quality of seismic interferometry.

In this research, I address the use of the attenuation in the weathered layer to reduce the noise from surface sources in data from surface receivers.

In seismic interferometry, the geophones are usually placed on the surface. It is known that there are multiple kinds of surface noise such as traffic noise, human activities, natural sources (such as wind and streams wave), and industry vibrations that could have defective effects on retrieved reflections. Due to the close proximity of the surface noise sources and the receivers, compared with deep source signal sources relative to distant receivers, the surface noise often dominates the recorded signal in land acquisition by a factor of 2 to 20. These surface noises, due to lack of attenuation in the path between them and the surface receivers, usually appear as high frequency coherent ambient noise. This would contaminate the body wave retrieved result. So, elimination of surface noise is critical on improving the retrieved results.

The weathered layer here refers to the unconsolidated uppermost layer of the earth. The weathered layer typically exhibits high porosity and lack of cementation. As a result, the bulk modulus is very low in this layer, which in turn results in low acoustic wave velocities. Usually, in the weathered layer, the anelastic effects have to be considered. Geophysicists use the quality factor Q to characterize the intrinsic attenuation of the layer. In the weathered layer, the quality factor is usually very low which means that this layer has a strong attenuation effect on seismic signals. Usually, the low velocity and attenuating effects of the weathered layer have negative impacts on data processing procedures. Therefore, the elimination of the defective effects or taking advantage of its low quality factor is a valuable topic for study. In this research, I use a visco-acoustic scheme for modeling, which means during the wave propagation, the mechanical energy will dissipate into heat energy. In the conventional receiver method where geophones are placed on the surface, the weathered layer acts as an attenuator of meaningful seismic signal, resulting in negative effects for a seismic survey; placing the receivers beneath the weathered layer may help.

In this research, I first observe the defective effect of surface noise by comparing the unmigrated stacked section of before and after adding surface noise. Then I put the

geophone below the weathered layer (initially with a high Q value) to observe the influence of top reflected multiples propagating downward to the buried geophones. In this model I also attempted to put hydrophones (which respond to the pressure field) together with geophones (which respond to displacement or velocity) to eliminate the top reflected multiples. Finally, I give the weathered layer a low quality factor and bury the geophones below the weathered layer to test the attenuation effect of the weathered layer on the surface noise.

2. Theory

In this section, basic mathematics used in passive seismic interferometry by cross-correlation and the main methodology used in this paper will be briefly introduced.

2.1 Seismic interferometry by cross-correlation

The term seismic interferometry, also known as Green's function retrieval, is a method that can generate new seismic response from different seismic observations recorded at different receivres. To gain a new seismic response, there are three mainstream methods in our field: cross-correlation, cross-coherence, and deconvolution. In this research, I used the cross-correlation method to retrieve the result.

Claerbout (1968) originally proposed a one-dimensional model. He proved that, by

using one-way transmission response from a source somewhere under the surface, a reflection response could be constructed. Using two-way reciprocity theorem, assuming an ideal homogeneous medium, and using just one impulsive source, Wapenaar and Fokkema (2006) proposed the relation below:

$$\hat{G}(x_B, x_A, \omega) + \hat{G}^*(x_B, x_A, \omega) \approx$$

$$\frac{2}{\rho c} \oint_S \hat{G}^*(x_A, x, \omega)\, \hat{G}(x_B, x, \omega) d^2x \qquad (1)$$

In the above relation, *S* refers to a closed surface and *x* is the coordinate of the source; x_A and x_B are the coordinates of the geophones put on the surface; ρ here refers to the bulk density and *c* is the acoustic velocity. The term $\hat{G}(x_B, x_A, \omega)$ refers to the Green's function received at x_B while the source located at x_A. And the term $\hat{G}^*(x_B, x_A, \omega)$ is the time reverse term of $\hat{G}(x_B, x_A, \omega)$. Equation (1) supposes the boundary *S* as a sphere and all of the rays are perpendicular to the sphere edge. In this relation, the dipole sources can be replaced with monopole sources. It should be mentioned, by making assumptions about things such as the ideal homogeneous medium, amplitude errors could surface in above relation, leading to spurious arrivals in seismic interferometry (Wapenaar and Fokkema 2006). However, even though the amplitude is unreliable, the signal phase would not be influenced by these errors, so *equation 1* is applicable in seismic interferometry.

Mutually uncorrelated sources occur when all noise sources and corresponding power spectra are different for all *x* coordinates, allowing one to define the noise signature as:

$$\langle \widehat{N}^*(x',\omega)\widehat{N}(x,\omega)\rangle = \delta(x-x')\hat{S}(\omega) \qquad (2)$$

In *equation 2*, the term $\widehat{N}(x,\omega)$ refers to the noise spectrum at coordinate *x* while term $\widehat{N}^*(x',\omega)$ is the time reverse term of $\widehat{N}(x,\omega)$. $\hat{S}(\omega)$ refers to the power spectrum of the source, and the symbol $\langle . \rangle$ refers to the calculation of spatial ensemble average. By combining *equation 1* and *equation 2*, a new equation can be derived:

$$\left\{\hat{G}(x_B,x_A,\omega) + \hat{G}^*(x_A,x_B,\omega)\right\}\hat{S}(\omega) \approx$$

$$\frac{2}{\rho c}\langle \hat{p}^{obs*}(x_A,\omega)\,\hat{p}^{obs}(x_B,\omega)\rangle \qquad (3)$$

Because the term $2/\rho c$ will have no influence on the retrieved phase of Green's function, we can rearrange the *equation 3* as:

$$\left\{\hat{G}(x_B,x_A,\omega) + \hat{G}^*(x_A,x_B,\omega)\right\}\hat{S}(\omega) \approx \langle \hat{p}^{obs*}(x_A,\omega)\,\hat{p}^{obs}(x_B,\omega)\rangle \qquad (4)$$

So we have:

$$\langle \hat{p}^{obs*}(x_A,\omega)\,\hat{p}^{obs}(x_B,\omega)\rangle = \oint_S \hat{G}^*(x_A,x,\omega)\,\hat{G}(x_B,x,\omega)\hat{S}(\omega)d^2x \qquad (5)$$

In above *equation 5*, the term $\hat{p}^{obs*}(x_A, \omega)$ refers to the time reverse of the observed wave field that was received at x_A. The term $\hat{p}^{obs}(x_B, \omega)$ refers to the observed wave field recorded at x_B. *Equation 4* shows the cross-correlation of seismic responses recorded at x_A and x_B can construct the wave field when a virtual source is located at one position while a receiver recording is at another position.

2.2 Methodology used in this paper

In this research, I do the numerical forward modeling using an open source code – 2D Finite-Difference Wave field Modelling (Thorbecke and Draganov, 2011) (downloaded from http://janth.home.xs4all.nl/Software/Software.html). This code is based on Seismic UN*X (SU). It calls SU commands to input, output, do binary options, processing, and display the seismic data.

The highlight of this package is that the author included some modeling features especially for passive seismic interferometry. In this package, there is a list of parameters defining the properties of random sources for seismic interferometry. *Figure 2.1* shows the parameters defining the properties of random sources in this package. Also, the availability of defining the quality factor by grid is another reason why I choose this package. In this package, one can define a global Q, a different Q for each layer, or even different Qs for different grid points that the user defines.

```
RANDOM SOURCE DEFINITION FOR SEISMIC INTERFEROMTERY:
  src_random=0 ..... 1 enables nsrc random sources positions in one modeling
  nsrc=1 ........... number of sources to use for one shot
  xsrc1=0 .......... left bound for x-position of sources
  xsrc2=0 .......... right bound for x-position of sources
  zsrc1=0 .......... left bound for z-position of sources
  zsrc2=0 .......... right bound for z-position of sources
  tsrc1=0.0 ........ begin time interval for random sources being triggered
  tsrc2=tmod ....... end time interval for random sources being triggered
  tactive=tsrc2 ..... end time for random sources being active
  tlength=tsrc2-tsrc1 average duration of random source signal
  length_random=1 ... duration of source is rand*tlength
  amplitude=0 ....... distribution of source amplitudes
  distribution=0 .... random function for amplitude and tlength 0=flat 1=Gaussian
  seed=10 ........... seed for start of random sequence
```

Figure 2.1. Random source definition for seismic interferometry in the code.

I input all the geo-model parameters, source parameters, receiver parameters, and other modeling parameters I designed into the script. After forward modeling, I obtained initial signal records recorded by all receivers. Then I chose certain receivers to be master traces, doing cross-correlation of them with all other traces. By cross-correlation, I obtain the virtual-shot gathers. After getting virtual-shot gathers, I

conducted conventional processing procedures on the data set —sort to CMP gathers, conduct velocity analysis, perform NMO correction, and stack each gather to obtain the final unmigrated stacked section. In this research, the main focus was on a method to increase the quality of the output traces and remove multiples. It was found that migration makes little contribution to the retrieved result, therefore migration was not applied to stacked sections. Likewise, time-depth conversion was not conducted, yielding deformed layers in the unmigrated stacked sections. Detailed illustration of these steps will be covered below in each section.

3. Numerical results

In this section, detailed forward modeling parameters and the processing steps will be described carefully. Comparisons will be made on the results and conclusions drawn.

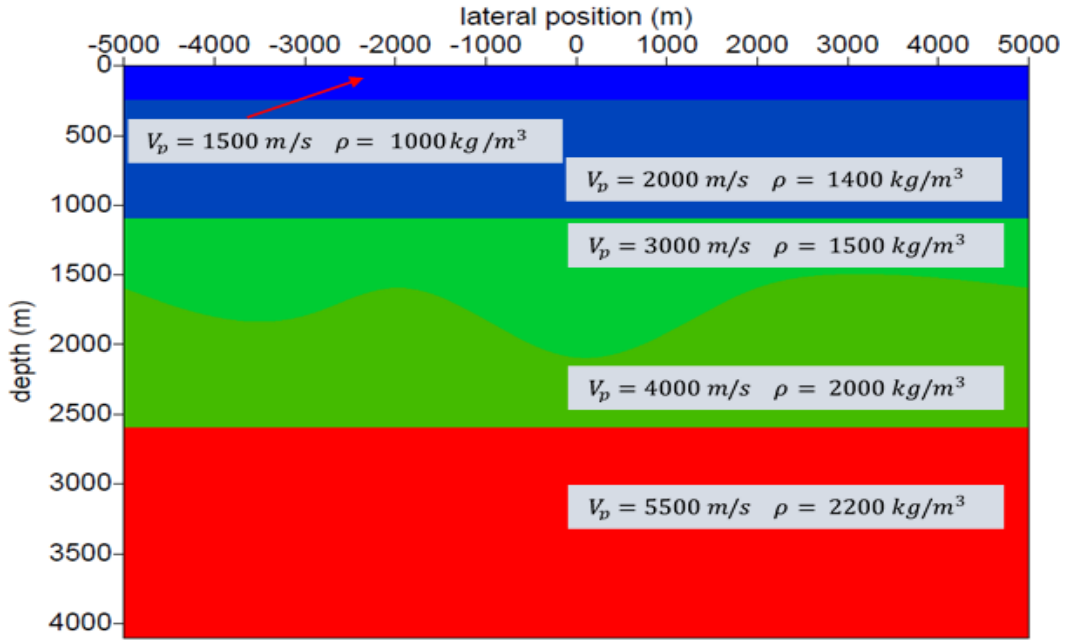

Figure 3.1. Topography and acoustic parameters of geo-model.

3.1 Surface noise influence

To observe the influence of surface waves on the output traces, an acoustic geo-model was used that assumes no attenuation. A 10,000m wide and 4,100m deep geo-model (*Figure 3.1*) was made. The uppermost layer, with a velocity of 1500 m/s, can be assumed to represent a water layer or a weathered layer. *Figure 3.2* shows the

locations of the surface receivers and the random source locations. In this figure, the red line with blue triangles shows the location of the surface receivers (range and interval will be describe below), and the black dots indicate the location of 8,000 random sources I used to generate the "deep source" (distant or deep) signals. These 8,000 sources were located randomly within the ranges of x: -5,000m-5,000m, y: 500m-4,090m and they were activated randomly during the time period of 0-120s. Because these deep source signals are intended to resemble those that have propagated from deep within the earth, most of the high frequency components would have been absorbed during propagation, and the maximum frequency of the deep source signal was set to 15Hz. *Figure 3.3* shows examples of 20 deep source signatures, with the 5th trace signature shown at a large scale. Its amplitude spectrum is shown in *Figure 3.3 c*.

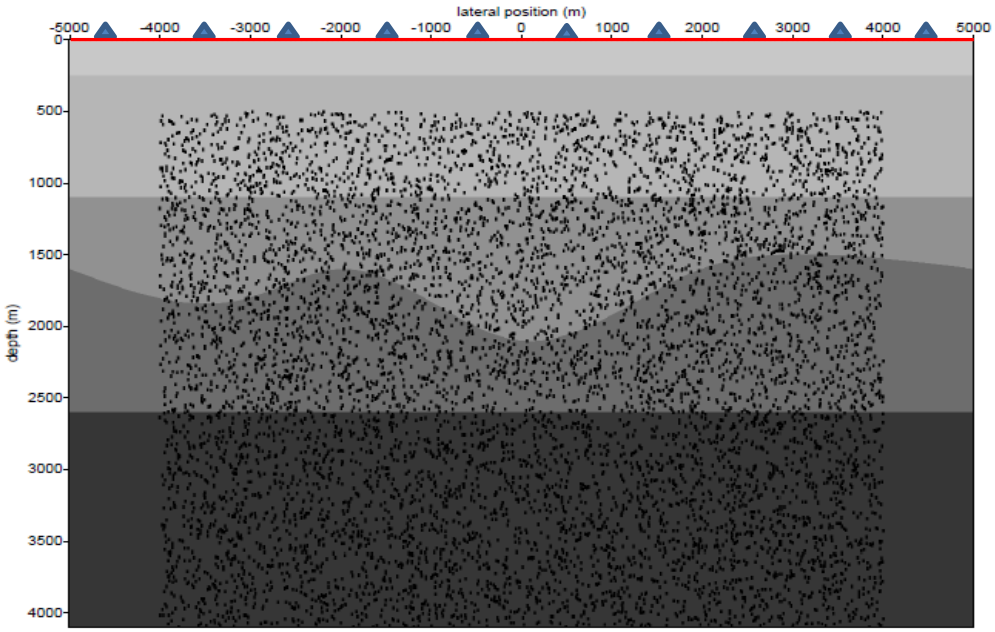

Figure 3.2. receivers and random sources location in geo-model (the red line with blue triangles show the vertical location of receivers (1001 receivers equally located from -5000m to 5000m with 10m interval) and the black dots indicate the location of 8000 random sources we use to model the deep source signal)

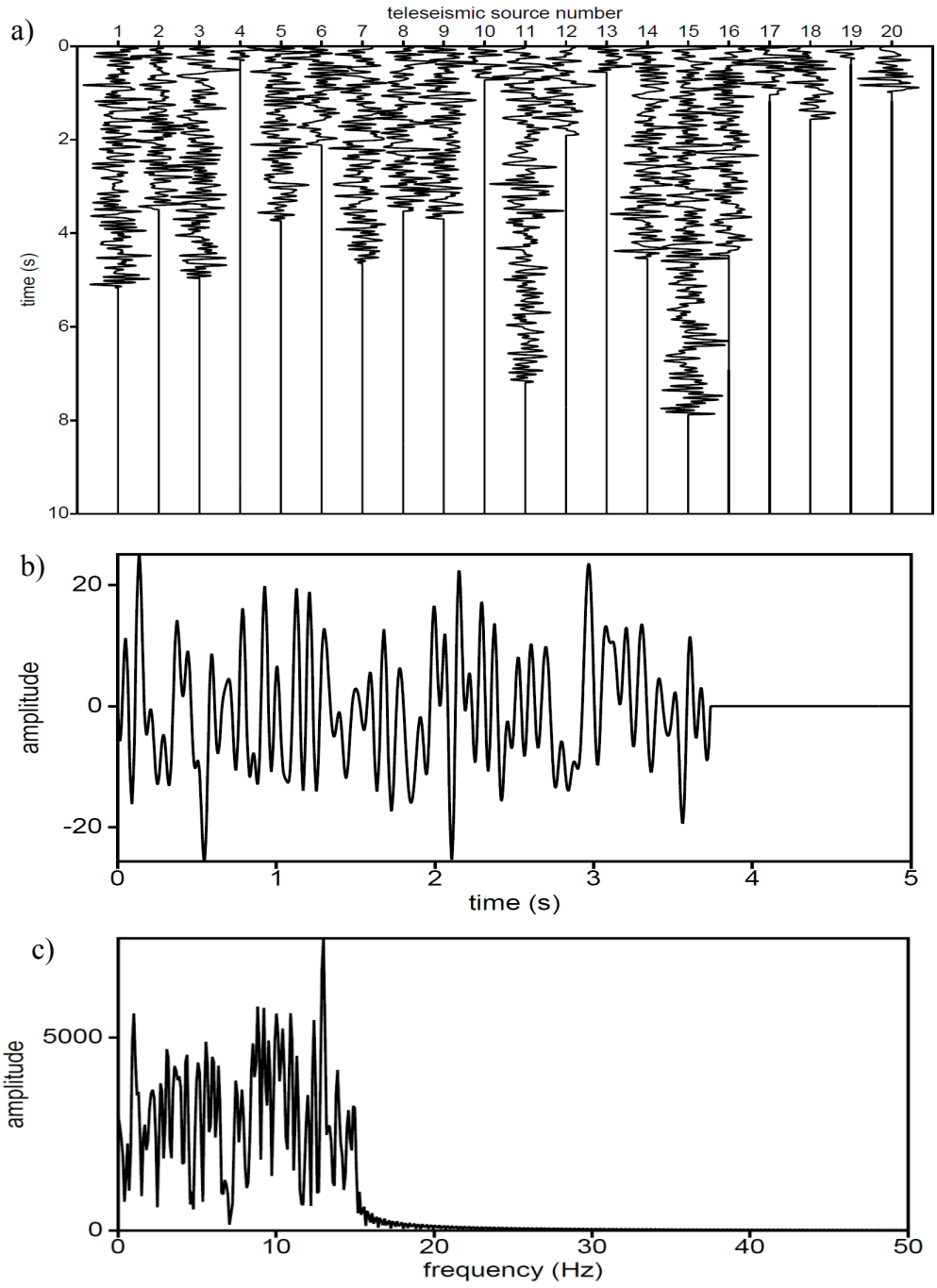

Figure 3.3. a) 20 deep sources' signatures, b) selected the 5th trace detail signature, c) its amplitude spectrum. One can see the maximum frequency is around 15Hz.

For the surface noise, 500 sources located randomly at the surface (x: 0-10000m, y:

0m) were chosen and activated randomly during 0-120s. Surface noise usually appears as high frequency coherent ambient noise, so the maximum frequency of surface noise was set to 30Hz. *Figure 3.4* shows 20 surface noise source signatures, with the selected 5th trace signature and its amplitude spectrum. Here I use 1,001 receivers located equably from 0-10,000m with 10m interval to collect the deep source signal and surface noise. Recording time is 120s. In this step the geophones were set as receivers on the surface (0m) as show in figure.

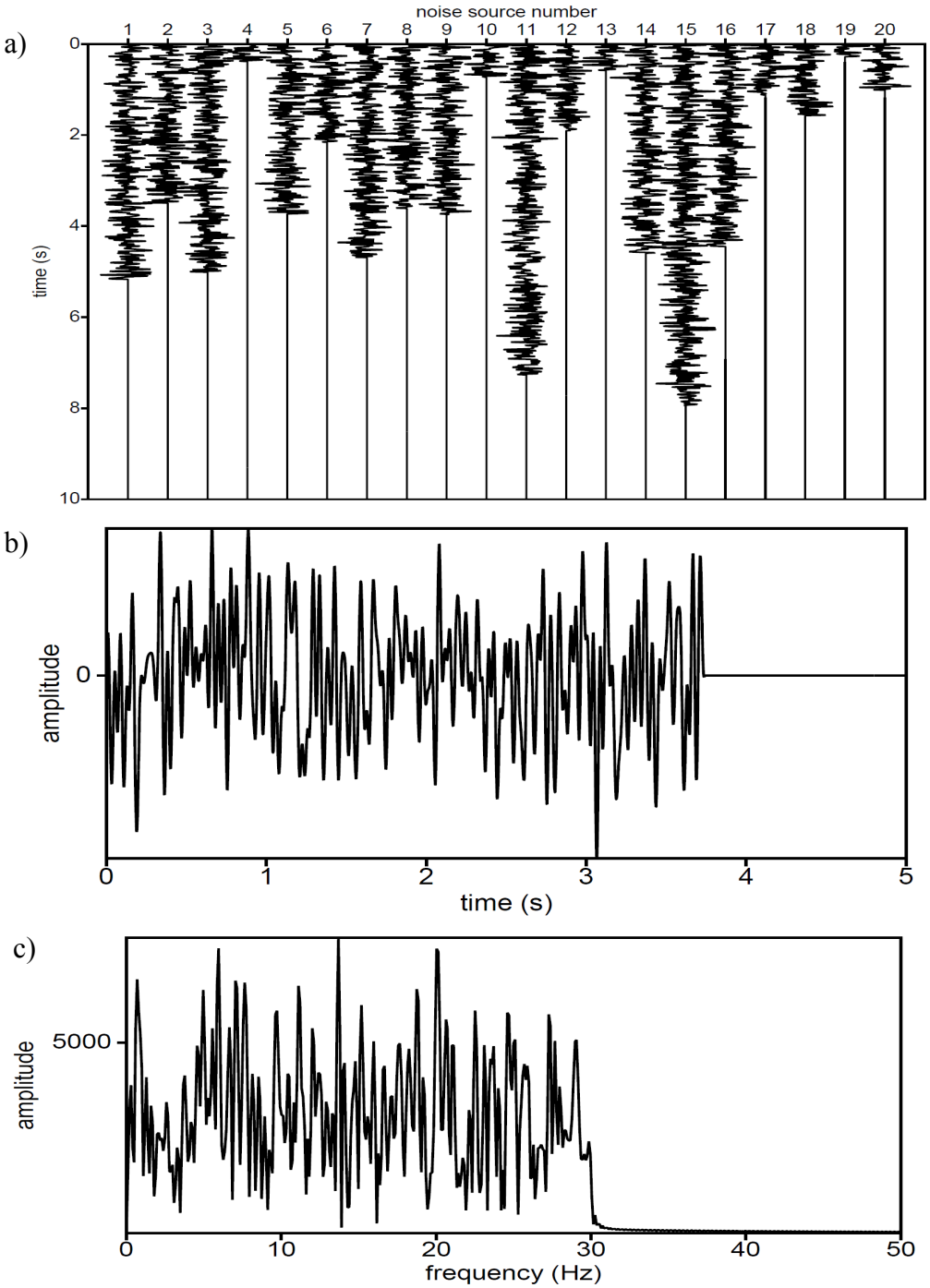

Figure 3.4. a) 20 surface noise sources' signatures, b) selected the 5th trace detail signature, c) its amplitude spectrum. One can see the maximum frequency is around 30Hz.

First, the deep source signal record without surface noise was modeled. *Figure 3.5*

shows the first four seconds of the 120-second long deep source signal record at all 1,001 geophones. Because there are so many overlapping signals, no recognizable information can be identified. Then, every 5th (1, 6, 11, 16, 21…) receiver was chosen as a master trace for cross-correlation with all other traces to generate the virtual shot gathers. After cross-correlation, there are 201 virtual shot gathers with a 50m shot interval, and each shot gather has 1000 traces with a 10m receiver interval. *Figure 3.6*

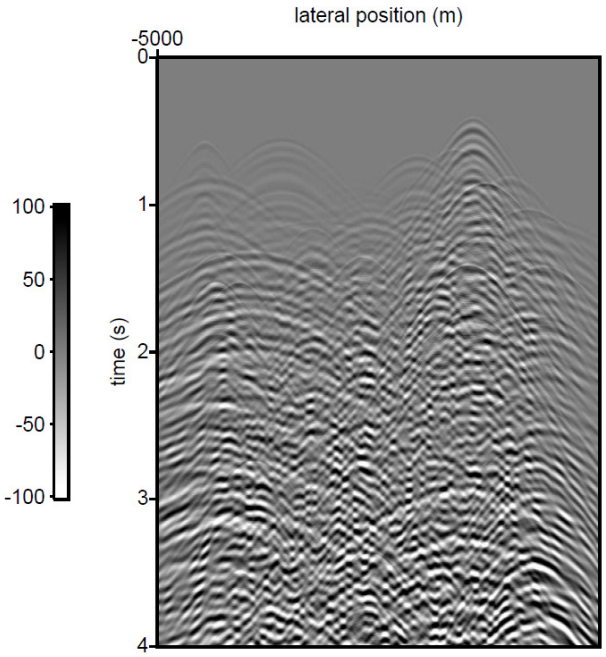

Figure 3.5. Initial deep source signal record of geophone from 0s to 4s.

shows three virtual shot gathers at the position of trace 301, 501, and 701. Clear reflections can be seen in the shot gathers. Because the third interface is curved, the peak of that hyperbola is not at the zero-offset position. After obtaining the virtual

source shot gathers, seismic headers were added to each trace for further processing, yielding separate shot gathers to be merged in one file. After merging and sorting to CMP gathers, velocity analysis and normal moveout (NMO) corrections were

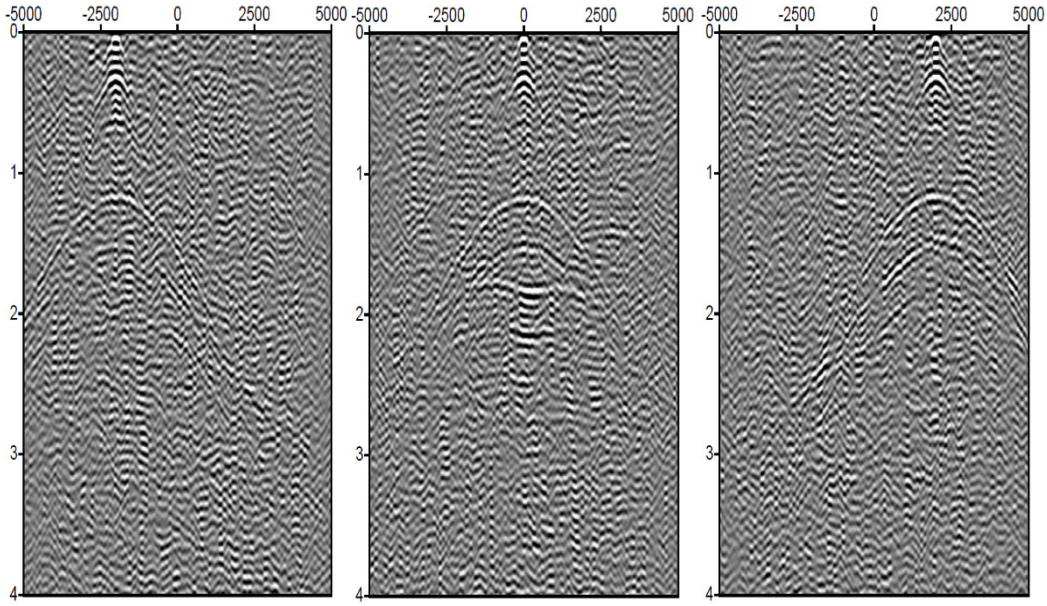

Figure 3.6. Three virtual shot gathers at the position of trace 301 (left), 501 (middle), and 701 (right).

conducted. For the velocity analysis, 100m CDP interval from 1,000 to 9,000 (the CDP range is 0-10,000) was chosen to conduct velocity analysis. In this paper, I conduct velocity analysis twice. The first velocity analysis was conducted using the CMP data processed from surface records, without noise, using the geophone records. The second velocity analysis (which is discussed later in this paper) was conducted on the section retrieved from geophone data recorded below the weathered layer (250m depth). *Figure 3.7* shows an example of the velocity analysis conducted on

CDP 1,000. One can see after NMO (in the third panel), the main reflections are roughly aligned. The table below lists the geo-model parameters and compares the picked velocities obtained in velocity analysis with RMS velocities computed from the model parameters.

From the *Table 3.1* one can observe that the picked velocities could roughly agree with the computed RMS velocity. So, this section is well stacked and the multiples are suppressed to some extent.

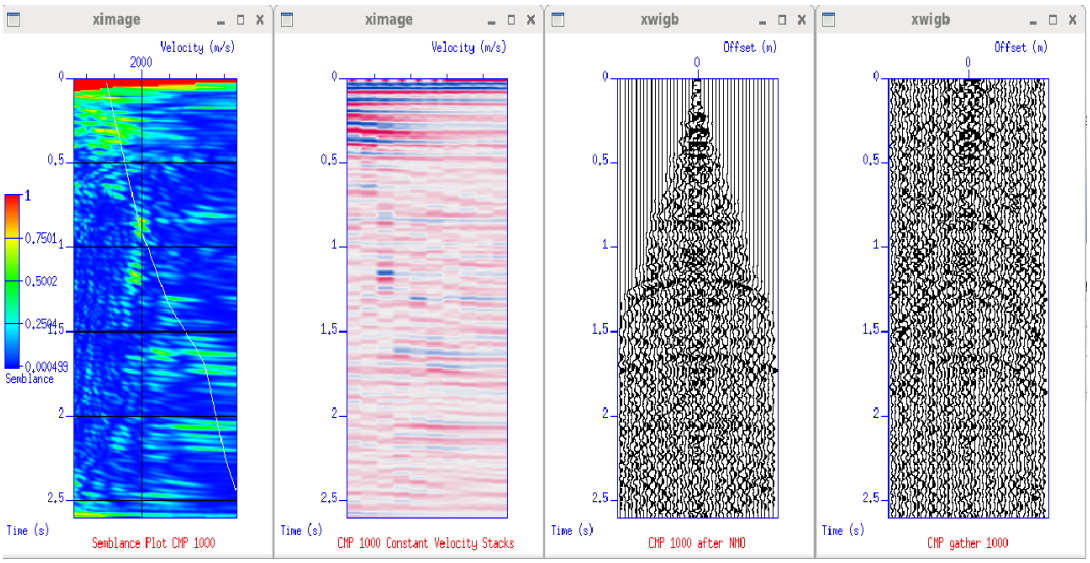

Figure 3.7. An example of the velocity analysis conducted on CDP 1000. The first panel: the color velocity analysis panel with the previous picks superimposed. The second panel: the CVS plot. The third panel: the CDP 1000 after NMO. The forth panel: a plot of the input CDP 1000.

Table 3.1. Geo-model parameters and comparison of the stacking velocity with calculated RMS velocity, the '' in table refers to approximate average values obtained because this model has a curved interface.*

Thickness of layer (m)	Depth to top of layer (m)	Time within the layer (s)	Interval Velocity (m/s)	Density (kg/m^3)	Picked velocity at the base reflector (m/s)	Computed RMS velocity at the base reflector (m/s)
250	0	0.33	1500	1000	1553	1500.0
850	250	0.85	2000	1400	1908	1873.7
500*	1100*	0.33*	3000	1500	2185*	2170.3*
1000*	1600*	0.50*	4000	2000	2711*	2742.0*

To better illustrate the reflections, the upper 0.6s is not displayed because of the high amplitudes associated with reflections at the base of the weathered layer (*Figure 3.8*). There is no AGC or time-dependent gain applied to this section. In the next model, a random surface noise source (500 random sources on the surface as defined above) was added. In Thorbecke and Draganov's code, two separate groups of sources cannot be applied in one run, so the surface noise record was modeled separately with the same geo-model parameters and receiver parameters. After obtaining the surface noise records, the binary add option in SU was used to add the surface noise records to the deep source signal records trace-by-trace. After creating this combined record, the same cross-correlation was performed on this record to get virtual shot gathers.

Then, after the conventional processing procedures described above were applied, the unmigrated stacked section with surface noise was obtained (I used the same group of stacking velocities because the model parameters and the receivers' positions

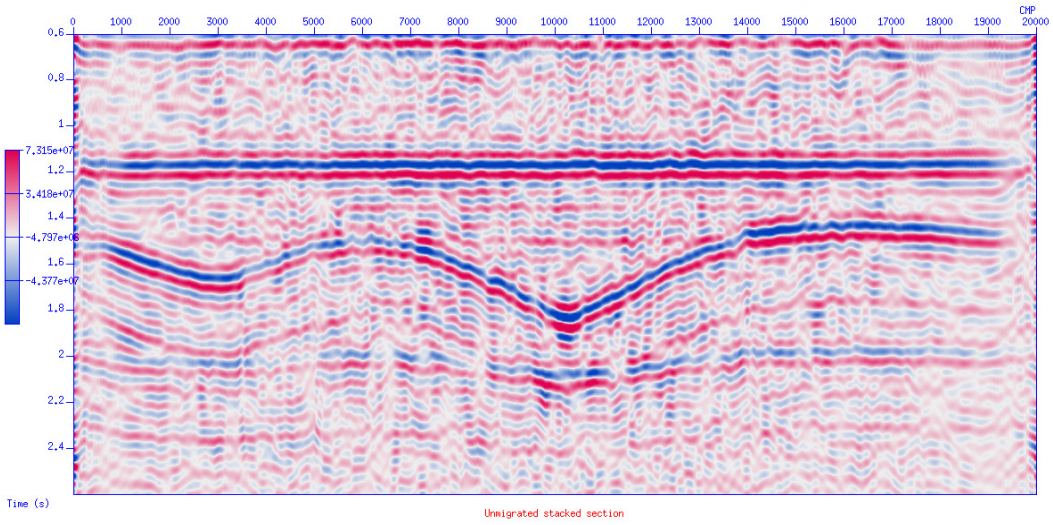

Figure 3.8. Umigrated stacked section without surface noise (received on the surface by geophones only).

remain the same). *Figure 3.9* shows the unmigrated stacked section of traces after adding noise. This section can be compared with the section without surface noise (*Figure 3.8*). The continuity of events in later sections are obviously broken by the addition of surface noise. It can be concluded that the surface noise as modeled here is detrimental to data quality.

3.2 Multiples generated by the free surface

In this portion of the study, a visco-acoustic numerical modeling code was used. To better illustrate the multiples, a high quality factor was initially set (1,500) for all the

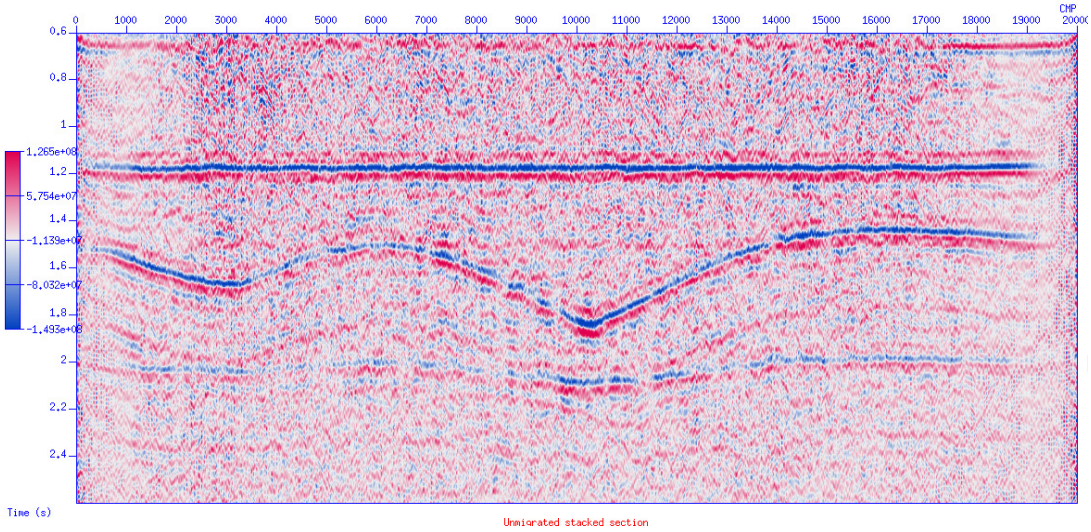

Figure 3.9. Umigrated stacked section after adding surface noise (received on the surface by geophones only).

layers. By using this high quality factor, reflections and multiples could be better observed. Low quality factors, appropriate weathered layer will have strong attenuation effect on top reflected multiples). In this step, the 1,001 receivers were put below the surface layer (at the depth of 250m) spaced at 10m intervals. The red line with blue triangles in *Figure 3.10* shows the receivers' position and the black dots show the 8,000 random deep sources' positions. Note that for buried receivers, additional arrivals will occur, representing the down going reflection from the uppermost, free, surface; in this study, we refer to these as "top reflected multiples". Given the model parameters, the top reflected multiple should follow each primary

by the two-way travel time in the weathered layer, or 0.33s (and integral multiples of that, for repeated bounces in the weathered layer).

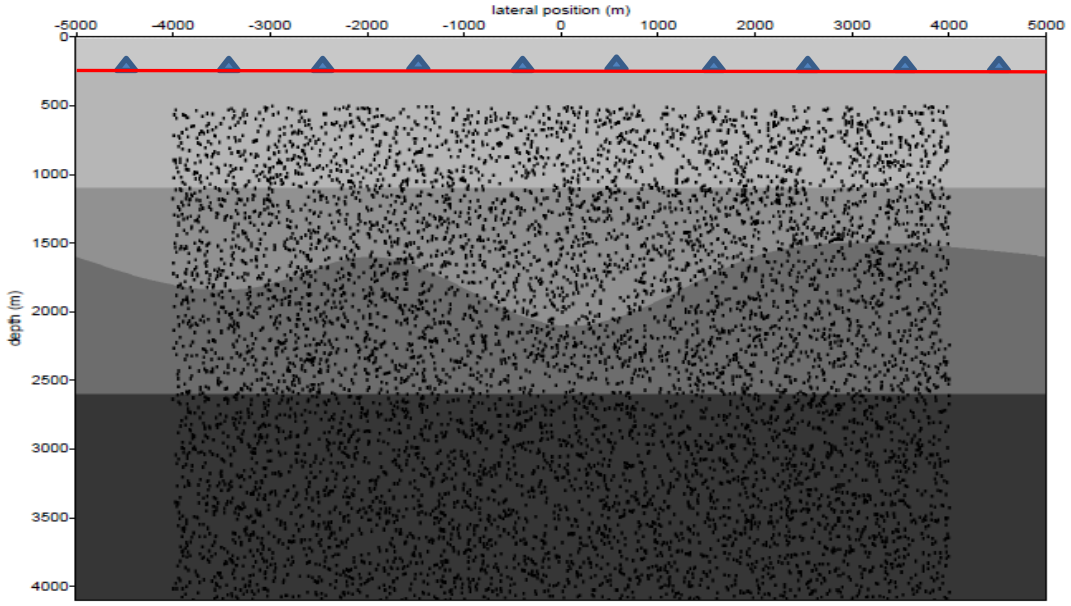

Figure 3.10. Receivers and random sources location in geo-model (the red line with blue triangles show the vertical location of receivers (below the weathered layer) (1001 receivers equally located from -5000m to 5000m with 10m interval) and the black dots indicate the location of 8000 random sources we use to model the deep source signal).

First, geophones were used to record the data. The steps to gain the initial records and to conduct the conventional processing procedures were identical to those described in *step 1*, while the velocity analysis was conducted a second time. Several attempts were made during this velocity analysis, but the results were not satisfactory apparently due to the strong energy in the top reflected multiples interfering with deeper arrivals. The quality factor of the weathered layer was then decreased to 30, and it was found that the energy in the multiples was sufficiently lower to enable

adequate tracking of the primary arrivals. The table below lists the geo-model parameters and compares the picked velocities obtained from the velocity analysis with RMS velocities computed from the model parameters.

Table 3.2. Geo-model parameters and comparison of the stacking velocity with calculated RMS velocity, the '' in table refer to approximate average values because this model have a curve interface.*

Thickness of layer (m)	Depth to top of layer (m)	Time within the layer (s)	Interval Velocity (m/s)	Density (kg/m^3)	Picked velocity at the base reflector (m/s)	Computed RMS velocity at the base reflector (m/s)
850	250	0.85	2000	1400	1984	2000
500*	1100*	0.33*	3000	1500	2411*	2323.4*
1000*	1600*	0.50*	4000	2000	2865*	2924.6*

From table above it can be seen that the picked velocities roughly agree with computed RMS velocity. This section is well stacked and the multiples are suppressed to some extent.

Figure 3.11 shows the unmigrated stacked section of the geophones result. Again, because the arrivals from bottom of the weathered layer (direct arrival at 0.166s), and the multiples within the weathered layer (every 0.33s later) are strong, times prior to 0.6s are not displayed. At around 0.85s a strong reflection is seen (indicated by the

arrow labeled A); this is the primary reflection of the second interface, at the base of the first layer beneath the weathered layer, at 1100m depth (see *Figure 3.1*). Because

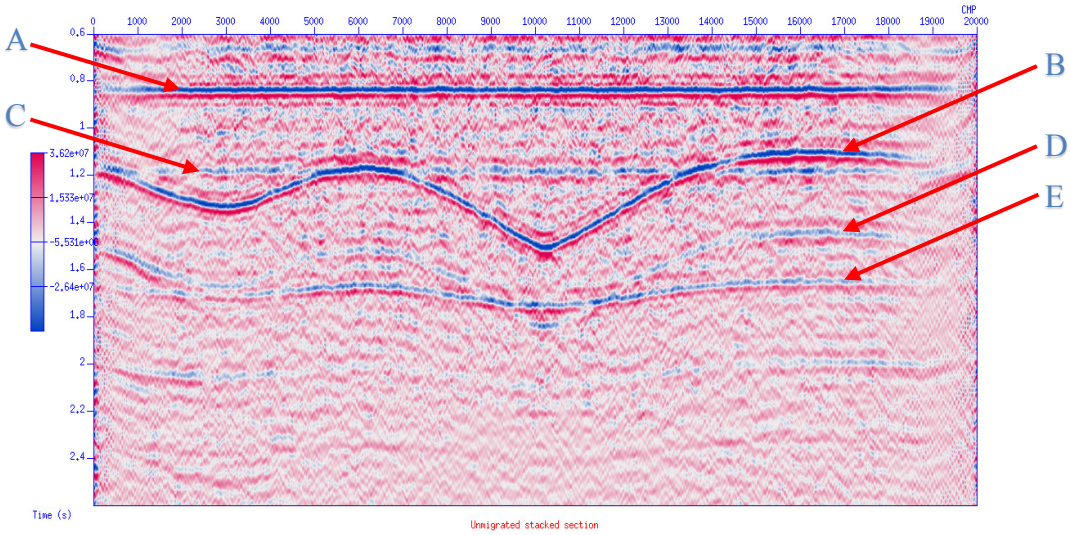

Figure 3.11. Unmigrated stacked section of geophones buried below the weathered layer (250m) with Q=1500.

the geophones are buried, the primary reflections all arrive about 0.33s earlier on this section than their counterparts on the surface-geophone section in *Figure 3.9*; that is, the modeling assumes that the virtual sources as well as the virtual receivers are buried at the same depths. At around 1.2s, two obvious reflections are seen: a strong curved event (arrow B) and a lighter straight event (arrow C). The curved event (arrow B) is the primary reflection of the third interface, at 1600m depth, and the lighter straight event (arrow C) is the top reflected multiple of the second straight interface, at 1100m depth. The arrival time of the reflection is at 0.85s and the arrival time of its top surface multiple is 1.19s, with a difference of about 0.33s, as expected (within

rounding). Similarly, it appears that the curved event at around 1.5s (arrow D) is the top reflected multiple of the primary reflection at 1.2s (arrow B). The bottom interface's reflection appears at around 1.67s (arrow E). In the geo-model, this interface was a straight horizontal interface, but in the unmigrated stacked section, this event appears to be curved due to the uneven thicknesses of overlying layers with different velocities. In this paper, the main focus is on finding a way to remove the top reflected multiples, therefore time-depth conversion was not performed to straighten this reflection.

In *Figure 3.11*, attention should be paid on the phase-sequence relation between the reflections and their corresponding top reflected multiples. The straight reflection at 0.85s (arrow A) and its multiple at 1.19s (arrow C) exhibit identical polarities. Because the geophones mainly measure the displacement of arrivals (velocity particle), upward displacement and downward displacement have different polarities. When the primary reflection reaches the geophones, it could be assumed that it first causes an upward displacement (as positive, shown in red), then a downward displacement (as negative, shown in blue), then upward (red). When this positive-negative-positive wavelet is reflected by the free surface, it will have a 180° phase change, altering the polarities to negative-positive-negative. But the wavelet

propagates to the receivers traveling downward, which means that the negative phase will cause an upward displacement at the geophones buried below the weathered layer. The displacement sequence of this top reflected multiple is upward-downward-upward again. Thus, the primary reflections exhibit the same phase as their multiples when collected by geophones.

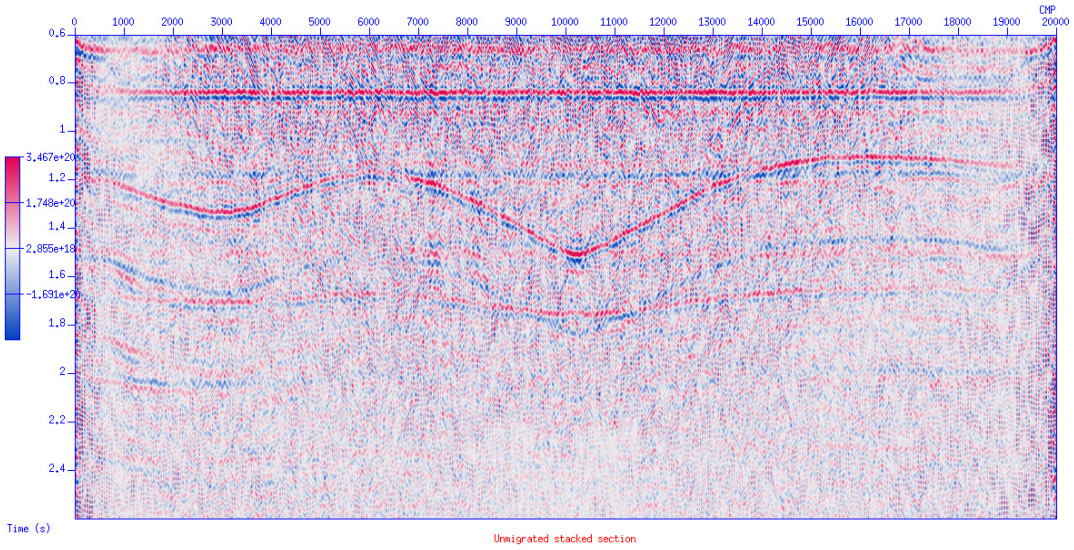

Figure 3.12. Unmigrated stacked section of hydrophones buried below the weathered layer (250m) with Q=1500.

Next, seismic interferometry was utilized to retrieve reflections from hydrophone data. *Figure 3.12* shows this result. While geophones measure the displacement (or particle velocity), most hydrophones are based on a piezoelectric transducer that generates a voltage when subjected to a pressure change. Hydrophones have two phases, compression and expansion, and they do not differentiate between upward or downward displacement. In this unmigrated stacked section, the positions of primary

reflections and their corresponding multiples are the same with those in the geophone result. However, the resulting quality is much poorer than observed in the geophone data in *Figure 3.11*, that is, the continuity of events in the hydrophone data is worse than that found in the geophone data in *Figure 3.11*.

Attention should be paid to the phase-sequence relation of primary reflections and their corresponding multiples in the hydrophone data. Though it is more difficult to identify the phase sequence of hydrophone data than that of the geophone data, in *Figure 3.12*, it can be observed that the primary reflections have the opposite phase sequence as their multiples. This is because the hydrophones measure the pressure changes. The phase is only changed by the free surface reflection, and not by the direction of propagation.

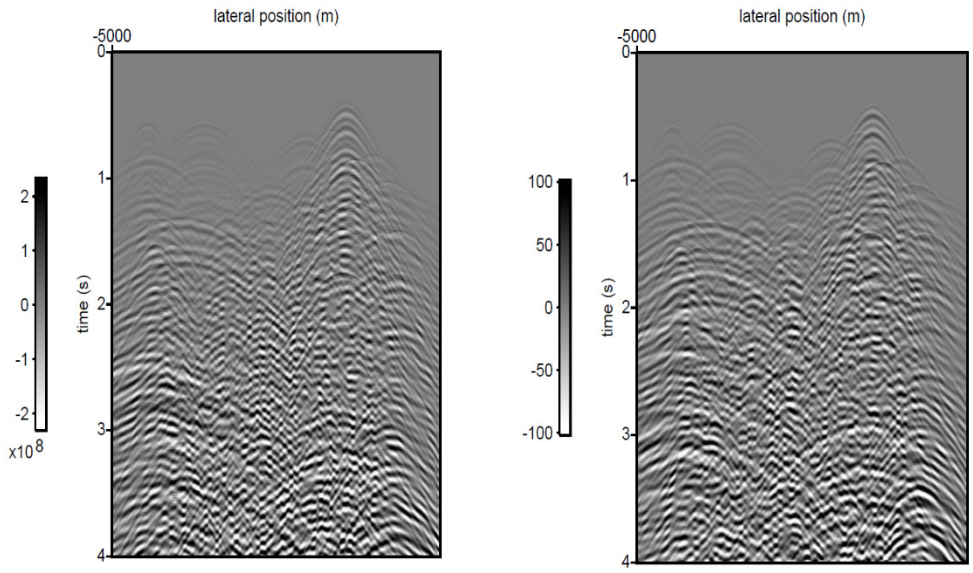

Figure 3.13. Amplitude comparison before RMS normalization of initial hydrophone record (left) and geophone record (right).

As is often done with ocean-bottom seismic data, subtraction of the two sections (hydrophone and geophone, assuming polarity conventions used here) should result in a section that does not include the top surface multiples. First, however, the phase and amplitude responses of the two sections must be normalized. Initially, we examine just the normalization of the amplitudes of the two sections.

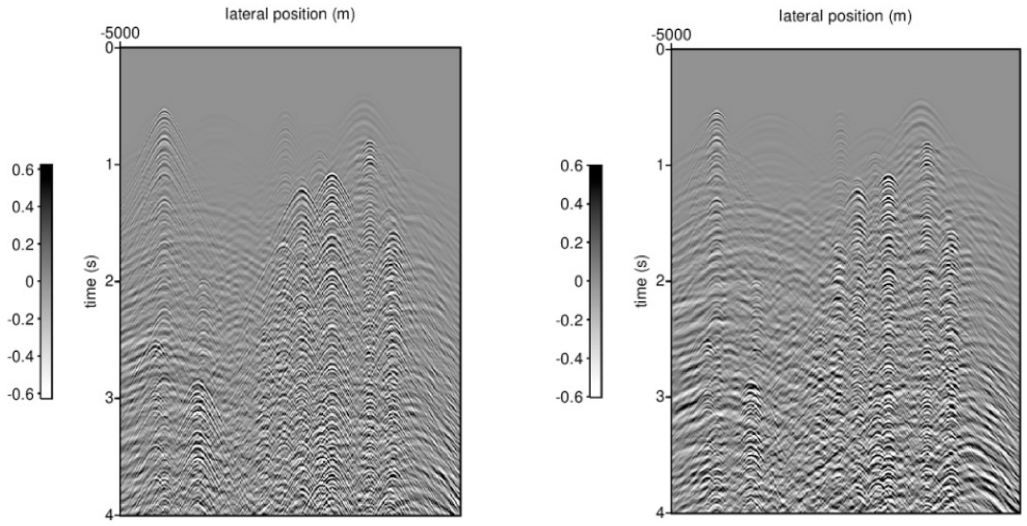

Figure 3.14. Amplitude comparison after RMS normalization of initial hydrophone record (left) and geophone record (right).

The removal can take place either prior to processing (simulating subtraction in the field) or after processing. Because the geophone and hydrophone measure two different physical parameters, the resulting magnitudes are different (and depend on the units used for each). If subtraction is performed directly on the two data sections before some kind of normalization is applied, the magnitude differences will overwhelm the results. *Figure 3.13* shows the initial signal record (before cross-correlation) before any kind of normalization, using the units that default in the program. To solve this problem, RMS (root mean square) normalization was conducted on both data sections separately, as can be seen in *Figure 3.14*, showing the initial signal record (before cross-correlation) after RMS normalization. The

legends on both records are similar now. After the RMS normalization, binary subtraction was performed on the geophone initial signal record (before cross-correlation) and the hydrophone initial signal record (before cross-correlation). Next, a combined signal record was obtained from the subtraction of the two records. Cross-correlation was conducted on this combined signal record and then regular processing procedures were conducted on this cross-correlated data. *Figure 3.15* shows the unmigrated stacked section processed from the subtracted section (the subtraction on initial records). Unfortunately, the multiple removal effect was not as effective as expected. It is hypothesized that this lack of complete multiple removal is mainly due

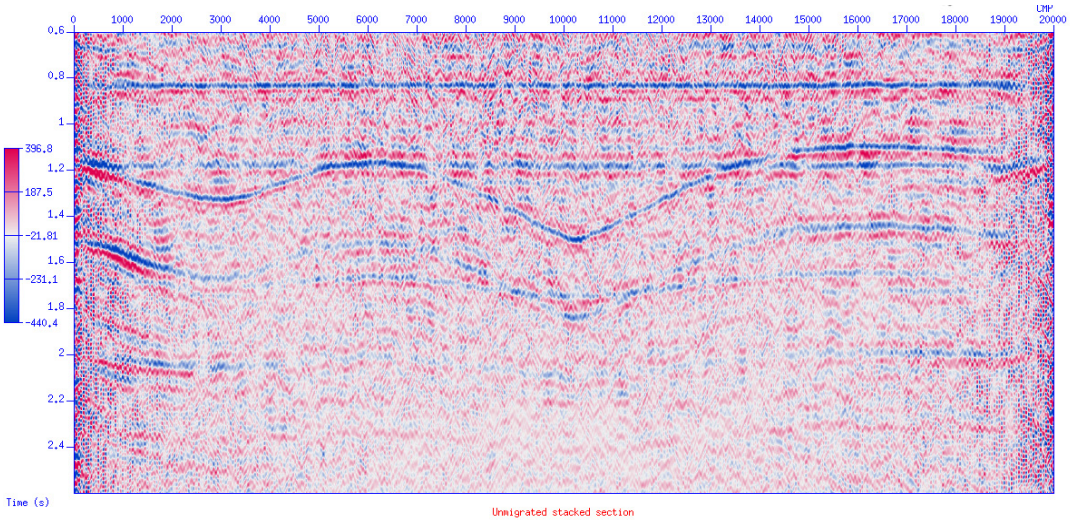

Figure 3.15. Unmigrated stacked section of geophone retrieved result minus hydrophones' buried below the weathered layer (250m) with Q=1500.

to the different response functions of the geophones and the hydrophones. In the code, if the geo-model is put in visco-acoustic scheme, it will model the pressure field and

velocity field separately. *Figure 3.16* shows the basic modeling equations used in visco-acoustic scheme modeling provided in this code's manual. If the geophone was chosen as receiver, the response of the particle velocity field would be recorded. If the hydrophone was chosen as receiver, the pressure field response would be recorded.

For a visco-acoustic medium the linearized equation of motion (Newton's second law) and equation of deformation (Hook's law) are :

$$\frac{\partial V_x}{\partial t} = -\frac{1}{\rho}\frac{\partial P}{\partial x} \tag{16}$$

$$\frac{\partial V_z}{\partial t} = -\frac{1}{\rho}\frac{\partial P}{\partial z} \tag{17}$$

$$\frac{\partial P}{\partial t} = -\frac{1}{\kappa}\frac{\tau_\varepsilon^p}{\tau_\sigma}\{\frac{\partial V_x}{\partial x} + \frac{\partial V_z}{\partial z}\} + r_p \tag{18}$$

$$\frac{\partial r_p}{\partial t} = -\frac{1}{\tau_\sigma}\left(r_p + (\frac{\tau_\varepsilon^p}{\tau_\sigma} - 1)(\frac{1}{\kappa})\{\frac{\partial V_x}{\partial x} + \frac{\partial V_z}{\partial z}\}\right) \tag{19}$$

Figure 3.16. Basic modeling equations used in visco-acoustic scheme modeling provided in this code's manual.

To resolve the issue of effectiveness in the multiple removal, two methods were formulated: 1) a transfer-function using the response of the geophone and the hydrophone could be created, then applied the transfer-function to the geophone data, and subtracted the transformed geophone data from the hydrophone data, or 2) predictive errors filtering (deconvolution) could be conducted.

Attempts have been made to design the transfer-function of the geophone data to match the hydrophone data. The methodology of designing the transfer-function is demonstrated below. In an ideal simplified scheme, the recorded signal could be expressed as:

$$s_{(t)} = w_{(t)} * r_{(t)},$$

In this equation, term $s_{(t)}$ is the recorded seismic signal, $w_{(t)}$ refers to the seismic wavelet, and $r_{(t)}$ is the receiver response function. '*' refers to the convolution operation. When Fourier transform was conducted on the above equation, the following formula was obtained:

$$S_{(f)} = W_{(f)}R_{(f)},$$

When subscripts for geophone and hydrophone were introduced, the formula was written as:

$$S_{G(f)} = W_{(f)}R_{G(f)},$$

$$S_{H(f)} = W_{(f)}R_{H(f)},$$

Subscript '*G*' refers to the geophones and '*H*' refers to the hydrophones. By combining the above two equations, the results are:

$$\frac{S_{G(f)}}{S_{H(f)}} = \frac{R_{G(f)}}{R_{H(f)}},$$

Then,

$$S_{H(f)} = \frac{R_{H(f)}}{R_{G(f)}} S_{G(f)}$$

$S_{G(f)}$ is the frequency spectrum of the geophones' recorded signal. $S_{H(f)}$ is the frequency spectrum of the hydrophones' recorded signal. $R_{G(f)}$ is the frequency spectrum of the geophones' response and $R_{H(f)}$ is that of the hydrophones' response. Now, the term $\frac{R_{H(f)}}{R_{G(f)}}$ is the transfer-function needed to match the hydrophone data with the geophone data.

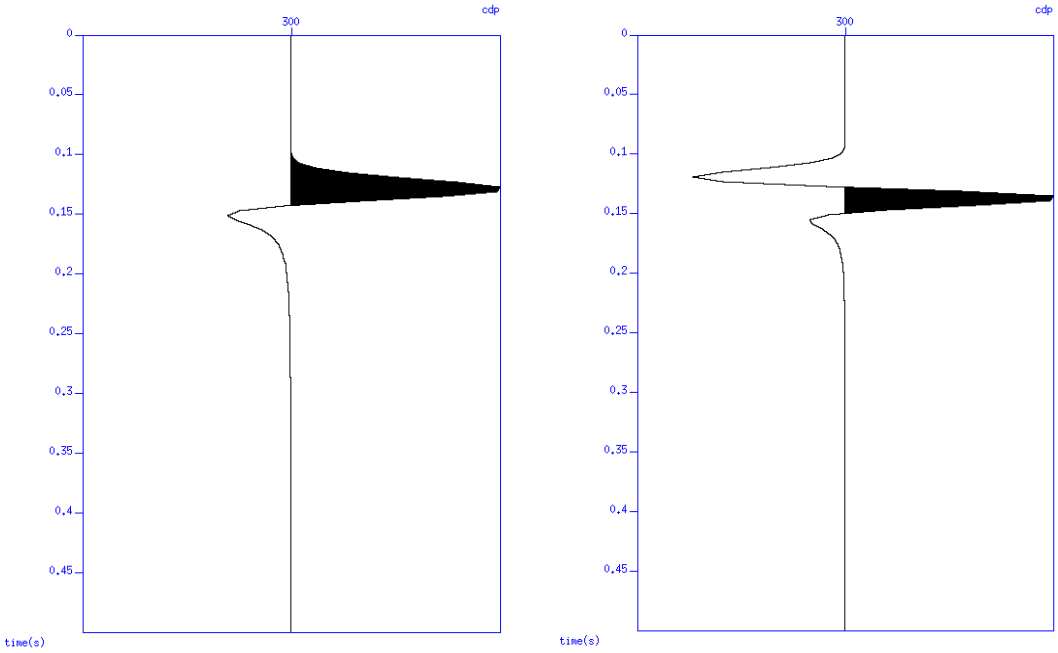

Figure 3.17. Comparison of single pulse record of geophone response (left) and hydrophone response (right).

To get the impulse responses of the geophones and the hydrophones, a simplified single-layer geo-model was built in acoustic scheme and a single pulse active source was placed in the middle of the surface with a 60Hz maximum frequency. The geophones and the hydrophones were combined, recording the single pulse signal that was produced. After windowing the geophones' and the hydrophones' traces down to

0-0.5s, single pulse signal data was obtained (*Figure 3.17*). Then Fourier transform was conducted on both traces (*Figure 3.18*) and 0s were added to the end of each trace to match the trace size of the synthetic seismic data. After Fourier transform, the transfer-function for geophones was obtained: $\frac{R_{H(f)}}{R_{G(f)}}$. After acquiring this transfer-function, Fourier transform was performed on the synthetic seismic data, and the transfer-function was applied to the seismic data in the frequency domain. After conducting inverse Fourier transform and taking the real part, the transformed geophone synthetic seismic data was retrieved.

To test the effectiveness of the transfer-function, we first apply it on the single pulse geophone signal. In *Figure 3.19*, the single pulse hydrophone signal and transformed single pulse geophone signal were compared side-by-side. It could be seen that the waveform of hydrophone signal and transformed geophone signal are the same. To confirm the effectiveness of the transfer-function, the difference of these two single

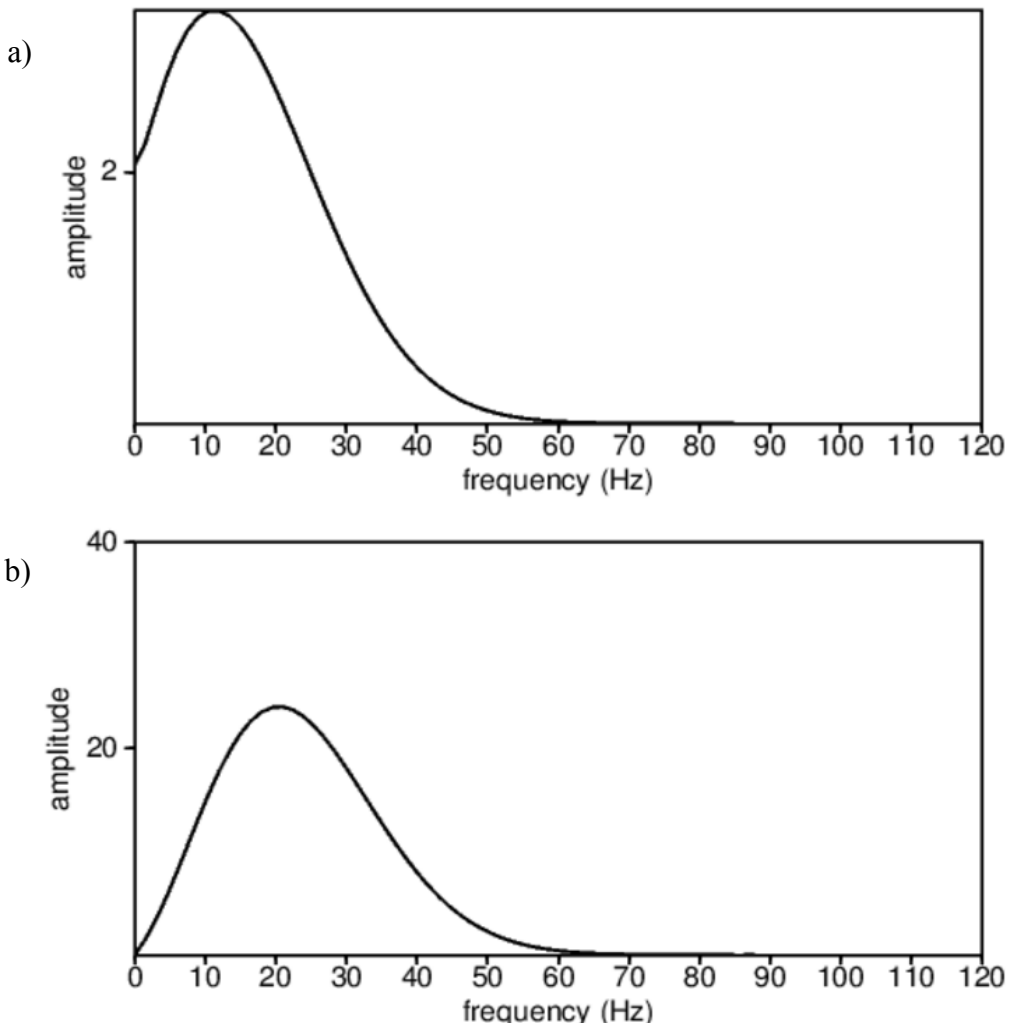

Figure 3.18. a) Frequency spectrum of geophone response, b) Frequency spectrum of hydrophone response.

pulse signal was calculated and the result is near zero (with the magnitude of 10^{-17} to 10^{-16}), which means that the transfer-function can work properly.

a)

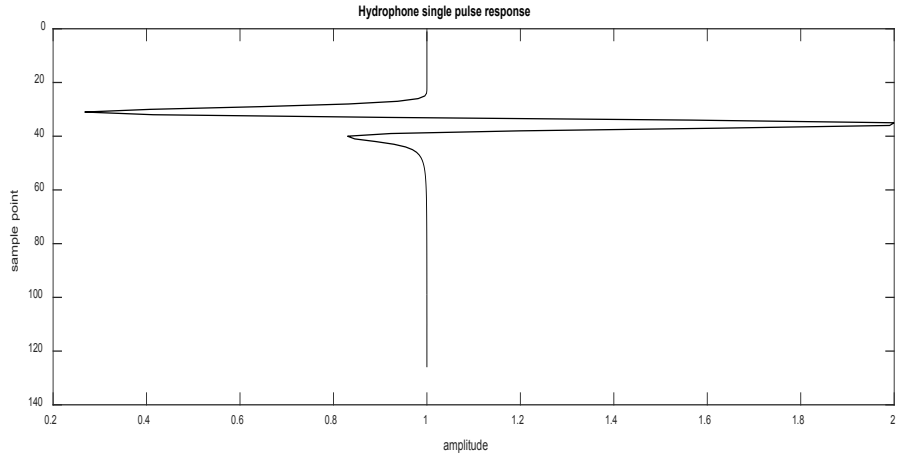

b)

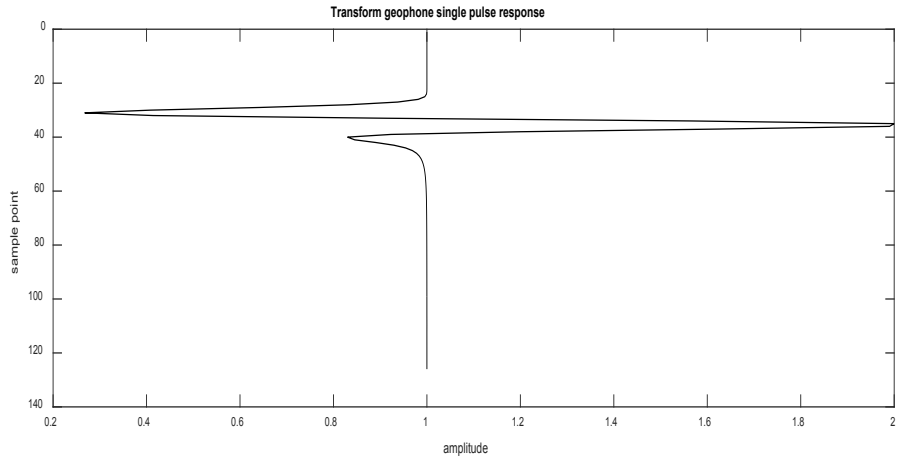

Figure 3.19. a) Single pulse response of hydrophone, b) single pulse response of transformed geophone.

When applying the transfer-function to the synthetic data, two methods were tested—applying the transfer-function on initial deep source record (before cross-correlation) (*Figure 3.20 (a)*) and on final stacked data (*Figure 3.20 (b)*). Comparing these two stacked sections, except for difference on scale, the result is almost the same.

Disappointingly, the application of the transfer-function had little influence on final result; it is not much better at multiple suppression than the original simple subtraction (after amplitude normalization).

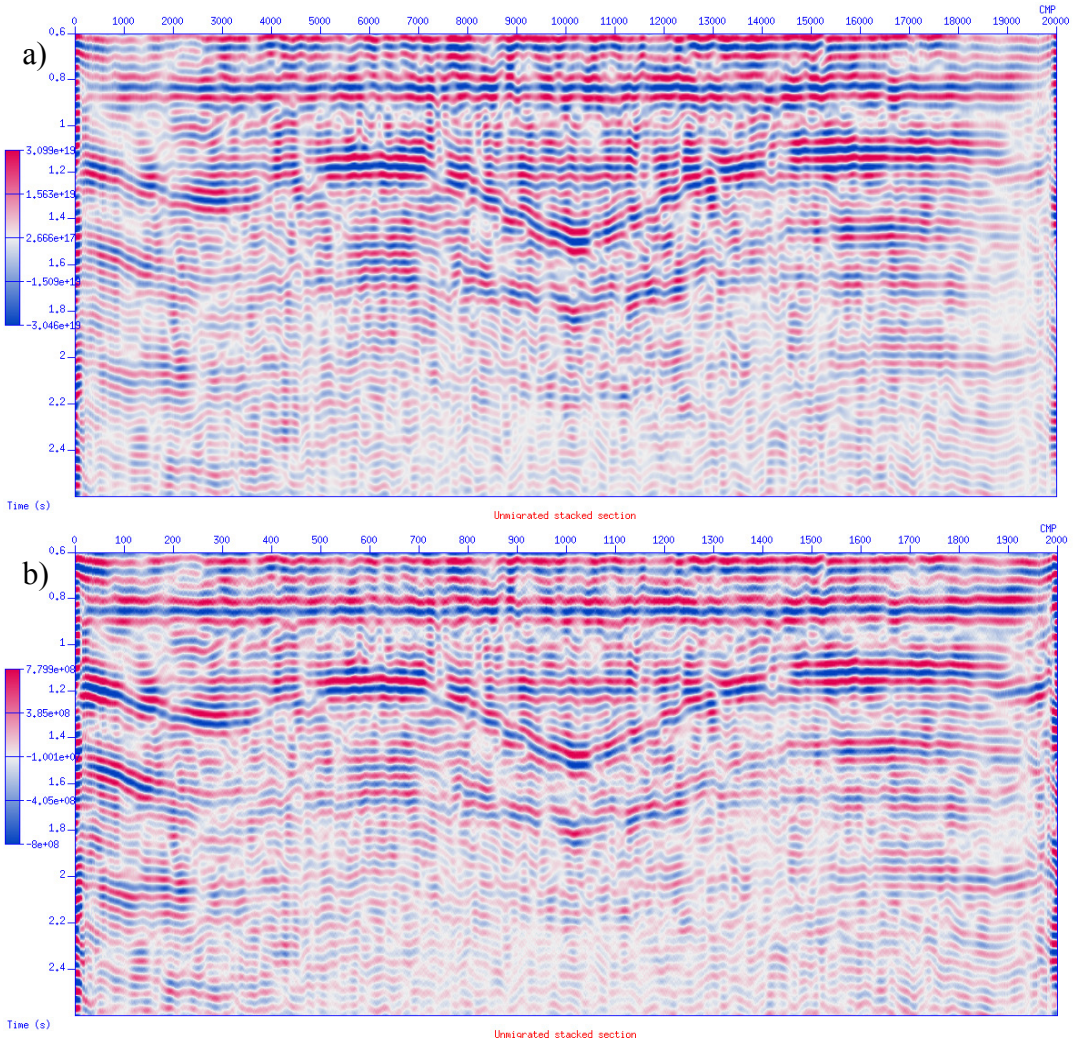

Figure 3.20. a) Stacked section of geophone response applying the transfer-function before cross-correlation, b) Stacked section of geophone response applying the transfer-function after stack

Figure 3.21 shows the stacked result of hydrophone data. Comparing the hydrophone result with the transformed geophone result (*Figure 3.20*), the difference in continuity

of reflections is obvious. The continuity of reflections in the hydrophone result is much poorer than that in the transformed geophone result. After RMS normalization, the transformed geophone result was subtracted from the hydrophone result (*Figure 3.22*). Due to the discontinuous nature of the hydrophone result, the multiple removing effect is not strong. At those few places with good event continuity (*Figure 3.23*), the multiple reflections were weakened but not removed thoroughly. The discontinuous nature of pressure transducer mainly comes from the response field of it. Pressure transducers are sensitive to pressure field. In pressure field, pressure transducers only have two phases—compress and expand, which are not sensitive to directions that waves come from. Based on this property, pressure transducers are more sensitive to surface noise that comes from different directions. So under the stronger destructive effects of surface noise, the events in pressure transducer result show worse continuity.

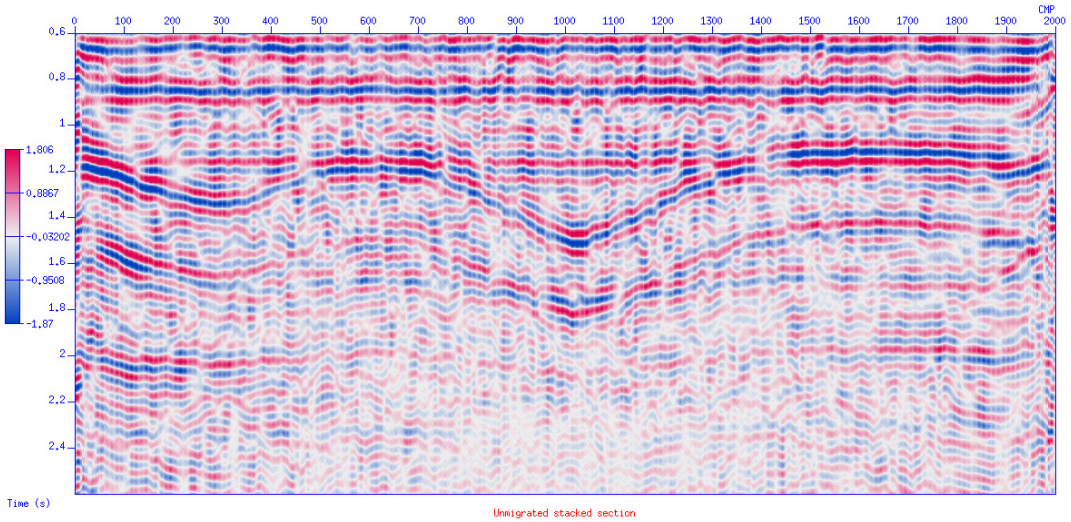

Figure 3.21. Subtracting transformed geophone stacked section from hydrophone stacked section.

Predictive deconvolution will be tested. But some concern comes out: the most interface in the geo-model are flat so that the predictive deconvolution may also remove some primaries of flat interface unless we simply take advantage of our knowledge of the model, and restrict the prediction to times appropriate for the top surface multiples.

3.3 Filtration effect of the weathered layer on surface noise

In this section, the quality factor of the weathered layer in the geo-model was set at 30, since a low quality factor means high dispersion and attenuation. This model reflects the real earth condition more accurately.

First, the geophones were put on the surface (x: 0-10,000m; y: 0m) with 10m interval.

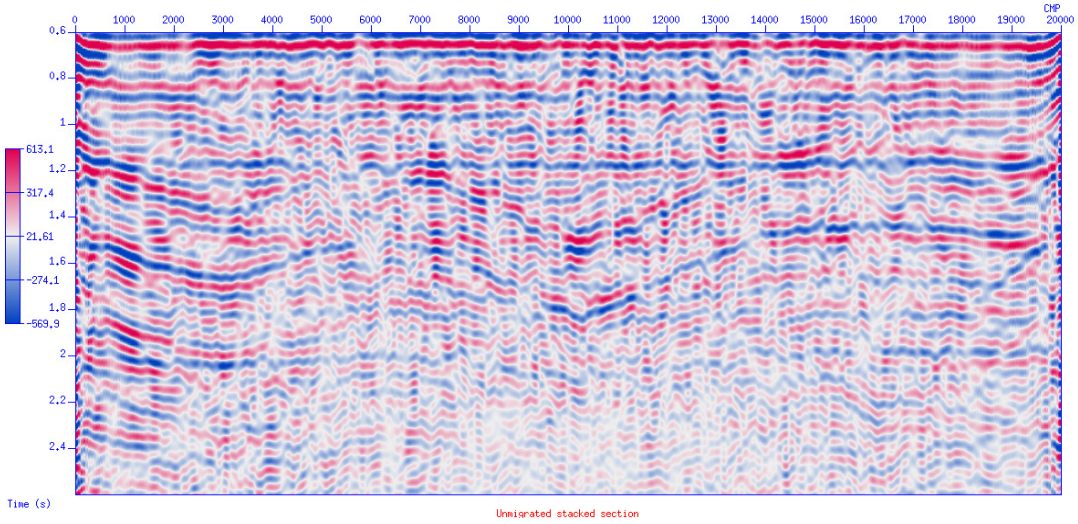

Figure 3.22. Stacked section of Hydrophone response.

The deep signal source was modeled by stimulating 8,000 volume random sources (stimulated randomly from 0s to 120s). Then the surface noise source was modeled by stimulating 500 random sources on the surface. After getting two sections, these

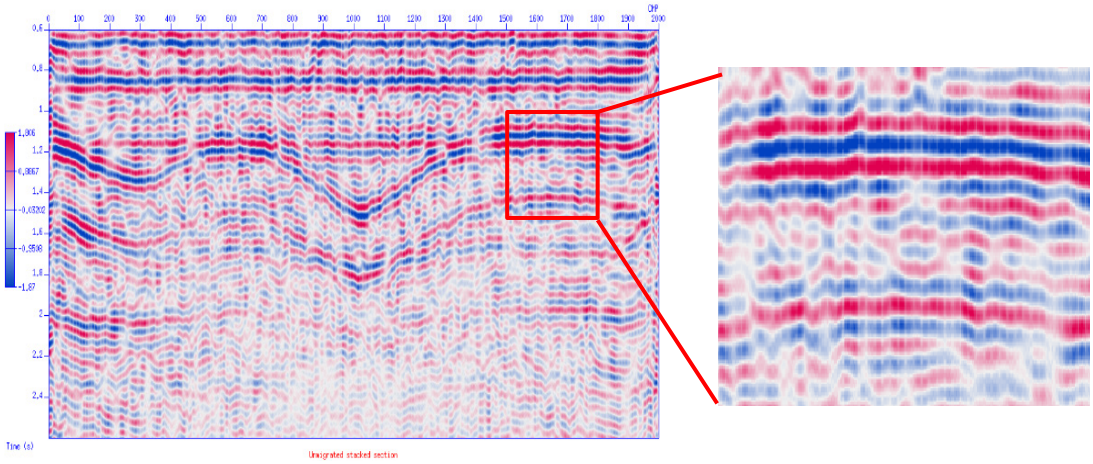

Figure 3.23. Insight detailed comparison of primary and its corresponding top reflected multiple.

two were added together getting a combined record. After cross-correlation, the shot

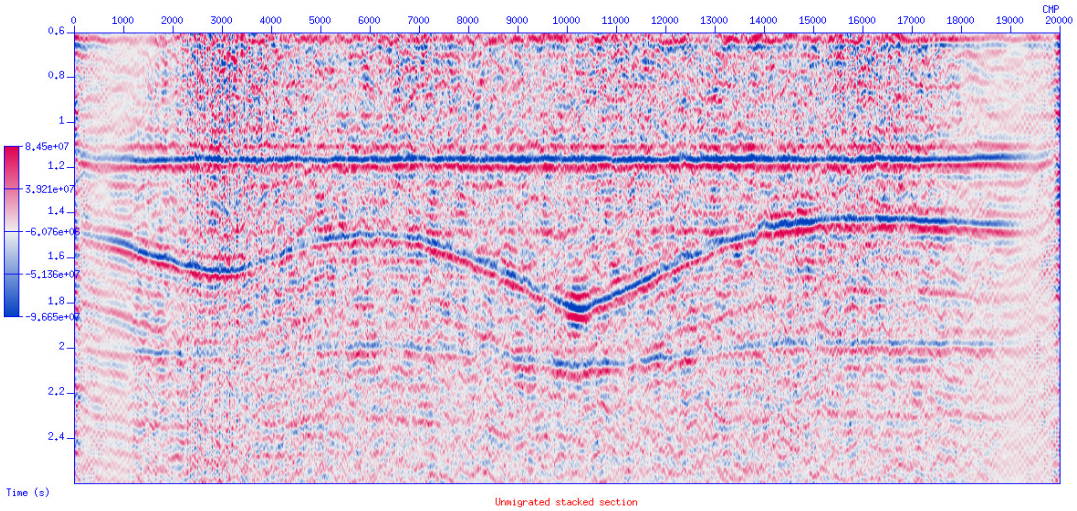

Figure 3.24. Unmigrated stacked section that retrieved by geophones put on surface, weathered layer Q=30.

gathers were retrieved and then being processed in Seismic Un*x, the unmigrated stacked section was obtained. *Figure 3.24* is the unmigrated stacked section that

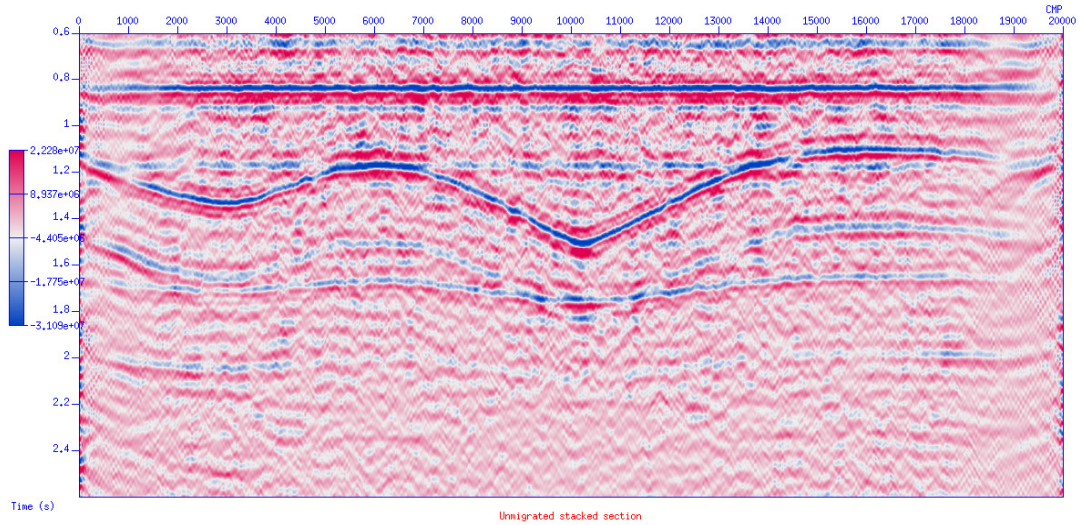

Figure 3.25. Unmigrated stacked section that retrieved by geophones put below the weathered layer with Q=30.

retrieved by geophones put on surface. The continuity of events in this section is poor.

Then all modeling parameters were kept the same but the geophones were buried at the base of the weathered layer (at depth of 250m). *Figure 3.25* shows the buried geophones retrieved section. By comparing this retrieved result with the result when the geophones were on the surface (*Figure 3.24*), it could be obviously observed that the continuity of events has been enhanced. But the by-product of burying the geophone is also obvious—the top reflected multiples appear, mixed with some of the primary reflections. Some of them even have tuning effect with primary reflections which may lead to mistakes when do further interpretation. Also, when comparing *Figure 3.25* with *Figure 3.11* that retrieved from geophone buried below the weathered layer with Q=1500, the low-Q model is improved over the high-Q model. So it appears that the weathered layer (with low quality factor) has a filtering effect on the surface noise, which may improve the quality of retrieved result compared with buried geophones in a high-Q environment.

4. Conclusions

Because it does not require using active sources, passive seismic interferometry is a cost-efficient seismic method in seismic exploration especially in some new seismic method such as 4D time lapse monitoring. But the resulting quality needs to be

improved. In this research, I explored the detrimental influence of surface noise and the influence of the weathered layer on the quality of seismic interferometry results. In step 1, the surface noise that destroys the continuity of events could be detected. When the geophones were placed on the surface, the weathered layer acts as an attenuator of signal. In this research, receivers are also placed below the weathered layer, and the imaging quality is improved significantly. The reflections are clearer to recognize and the continuity of the events is improved. However, the by-product is some misleading top reflected multiples. To remove these multiples, I tried a new method for land-based acquisition: combining the geophone and the hydrophone results. But due to the discontinuous nature of the hydrophone result, the multiple removing effect is not ideal. For a better result, further techniques that could enhance the correlation of the geophone stacked result and the hydrophone result should be conducted, such as trace smoothing and dip-oriented trace merging. So it has been demonstrated that by burying the geophones below the weathered layer, the detrimental effect of surface noise could be eliminated to a certain extent, and that the quality of SI retrieved result can be improved significantly.

5. References

Bakulin, A. and Calvert, R., 2006. The virtual source method: Theory and case study. Geophysics, 71(4), pp.SI139-SI150.

Boullenger, B., Verdel, A., Paap, B., Thorbecke, J. and Draganov, D., 2015, April. Time-lapse CO2 monitoring using ambient-noise seismic interferometry: a feasibility study from Ketzin, Germany. In EGU General Assembly Conference Abstracts (Vol. 17, p. 1460).

Campillo, M. and Paul, A., 2003. Long-range correlations in the diffuse seismic coda. Science, 299(5606), pp.547-549.

Curtis, A., 2009, January. Source-receiver seismic interferometry. In 2009 SEG Annual Meeting. Society of Exploration Geophysicists.

Draganov, D., Campman, X., Thorbecke, J., Verdel, A. and Wapenaar, K., 2009. Reflection images from ambient seismic noise. Geophysics, 74(5), pp.A63-A67.

Draganov, D., Wapenaar, K. and Thorbecke, J., 2004. Passive seismic imaging in the presence of white noise sources. The Leading Edge, 23(9), pp.889-892.

Draganov, D., Wapenaar, K. and Thorbecke, J., 2006. Seismic interferometry: Reconstructing the earth's reflection response. Geophysics,71(4), pp.SI61-SI70.

Draganov, D., Wapenaar, K., Mulder, W., Singer, J. and Verdel, A., 2007. Retrieval of reflections from seismic background - noise measurements.Geophysical Research Letters, 34(4).

Forghani, F. and Snieder, R., 2010. Underestimation of body waves and feasibility of surface-wave reconstruction by seismic interferometry. The Leading Edge, 29(7), pp.790-794.

Lobkis, O.I. and Weaver, R.L., 2001. On the emergence of the Green's function in the correlations of a diffuse field. The Journal of the Acoustical Society of America, 110(6), pp.3011-3017.

Rickett, J. and Claerbout, J., 1999. Acoustic daylight imaging via spectral factorization: Helioseismology and reservoir monitoring. The leading edge,18(8), pp.957-960.

Scherbaum, F., 1987. Seismic imaging of the site response using microearthquake recordings. Part II. Application to the Swabian Jura, southwest Germany,

Seismic network. Bulletin of the Seismological Society of America, 77(6), pp.1924-1944.

Shapiro, N.M. and Campillo, M., 2004. Emergence of broadband Rayleigh waves from correlations of the ambient seismic noise. Geophysical Research Letters, 31(7).

Snieder, R. and Şafak, E., 2006. Extracting the building response using seismic interferometry: Theory and application to the Millikan Library in Pasadena, California. Bulletin of the Seismological Society of America,96(2), pp.586-598.

Snieder, R., 2004. Extracting the Green's function from the correlation of coda waves: A derivation based on stationary phase. Physical Review E,69(4), p.046610.

Thorbecke, J.W. and Draganov, D., 2011. Finite-difference modeling experiments for seismic interferometry. Geophysics, 76(6), pp.H1-H18.

van Manen, D.J., Curtis, A. and Robertsson, J.O., 2006. Interferometric modeling of wave propagation in inhomogeneous elastic media using time reversal and reciprocity. Geophysics, 71(4), pp.SI47-SI60.

van Manen, D.J., Robertsson, J.O. and Curtis, A., 2005. Modeling of wave

propagation in inhomogeneous media. Physical Review Letters, 94(16), p.164301.

Van Tiggelen, B.A., 2003. Green function retrieval and time reversal in a disordered world. Physical review letters, 91(24), p.243904.

Wapenaar, K., 2003. Synthesis of an inhomogeneous medium from its acoustic transmission response. Geophysics, 68(5), pp.1756-1759.

Wapenaar, K., 2004. Retrieving the elastodynamic Green's function of an arbitrary inhomogeneous medium by cross correlation. Physical review letters, 93(25), p.254301.